Utilizing UV-LED pulse width modulation on TiO_2 advanced oxidation processes to enhance the decomposition efficiency of pharmaceutical micropollutants

Robert Liang, Jocelyn C. Van Leuwen, Leslie M. Bragg, Maricor J. Arlos, Lena C.M. Li Chun Fong, Olivia M. Schneider, Ivana Jaciw- Zurakowsky, Azar Fattahi, Peng Peng, Mark R. Servos, Y. Norman Zhou

PII: S1385-8947(18)32537-3
DOI: https://doi.org/10.1016/j.cej.2018.12.065
Reference: CEJ 20605

To appear in: *Chemical Engineering Journal*

Received Date: 5 December 2017
Revised Date: 22 October 2018
Accepted Date: 13 December 2018

Please cite this article as: R. Liang, J.C. Van Leuwen, L.M. Bragg, M.J. Arlos, L.C.M. Li Chun Fong, O.M. Schneider, I. Jaciw- Zurakowsky, A. Fattahi, P. Peng, M.R. Servos, Y. Norman Zhou, Utilizing UV-LED pulse width modulation on TiO_2 advanced oxidation processes to enhance the decomposition efficiency of pharmaceutical micropollutants, *Chemical Engineering Journal* (2018), doi: https://doi.org/10.1016/j.cej.2018.12.065

Utilizing UV-LED pulse width modulation on TiO_2 advanced oxidation processes to enhance the decomposition efficiency of pharmaceutical micropollutants

Robert Liang[1,2,3*], Jocelyn C. Van Leuwen[1], Leslie M. Bragg[3], Maricor J. Arlos[3], Lena C. M. Li Chun Fong[1], Olivia M. Schneider[1], Ivana Jaciw- Zurakowsky[1,2], Azar Fattahi[1,2], Peng Peng[4], Mark R. Servos[3], and Y. Norman Zhou[1,2]

[1]Centre for Advanced Materials Joining, Department of Mechanical and Mechatronics Engineering, University of Waterloo, Waterloo, Ontario, Canada, N2L 3G1

[2]Waterloo Institute of Nanotechnology, University of Waterloo, Waterloo, Ontario, N2L3G1

[3]Department of Biology, University of Waterloo, Waterloo, ON, Canada

[4]School of Mechanical Engineering and Automation, [4] International Research Institute for Multidisciplinary Science, Beihang University, 37 Xueyuan Rd, Beijing, 100191

[*]**Corresponding Author**

Centre for Advanced Materials Joining, Department of Mechanical and Mechatronics Engineering, University of Waterloo, Waterloo, Ontario, Canada, N2L 3G1

Tel: +1-519-888-4567 x33326

Email: rliang@uwaterloo.ca

Alternative Email: rliang66@gmail.com

ABSTRACT

The presence of pharmaceutical and personal care products (PPCPs) in aquatic systems has been a growing cause for concern. Advanced oxidation processes such as UV/TiO_2 (ultraviolet light/ Titanium Dioxide) can break down PPCPs into smaller constituents, reducing the pharmaceutical activity. However, this process is limited by low photonic efficiency under UV systems. Controlled periodic illumination (CPI) is a promising solution to overcome the issues concerning low photonic efficiencies. Using a CPI controlled UV-LED/TiO_2 process, a mixture of eighteen PPCP compounds were analyzed for their degradation removal on porous titanium – titanium dioxide (PTT) substrates. The kinetic rate constants of PPCPs may be analyzed using multiple regression analysis with parameters such as net charge at experimental pH, solubility, and molecular weight. Negatively charged PPCP compounds were found to have the highest removal compared to neutral and positively charged compounds due to electrostatic attraction forces. Decreasing the duty cycle under CPI or the UV-LED illumination period did not significantly change the individual and cumulative PPCP compound removal, suggesting that the CPI controlled UV-LED/TiO_2 processes using PTT substrates were effective in reducing energy requirements without sacrificing removal performance.

Keywords: titanium dioxide, emerging contaminants, controlled periodic illumination, advanced oxidation process, pharmaceutical and personal care products, Parrondo's paradox

1. INTRODUCTION

Pharmaceutical and personal care products (PPCPs) have been an increasing subject of interest with respect to their environmental impact. The influx of attention from the general population of the possible negative effects of various bioactive pharmaceuticals on both drinking water and wastewater has driven scientists to explore treatment options that render pharmaceuticals inactive [1]. A promising treatment option involves using UV-LED (ultraviolet-light emitting diode) light irradiation with titanium dioxide photocatalysts, which have been shown to degrade various emerging contaminants such as dyes and pharmaceuticals [2–9].

Advanced oxidation processes (AOPs) such as ozone (O_3) and hydrogen peroxide (H_2O_2) are effective in treating organic contaminants but require a constant supply of chemical oxidants [10–14]. The use of UV-LEDs and photocatalytic materials, such as TiO_2, can be used to drive AOPs with a renewable oxidant source. A natural or artificial radiation source, such as UV-LEDs, of enough energy will generate electron-hole pairs that can participate in redox reactions. These redox reactions can decompose small molecules such as organic micropollutants, driving AOPs [7,8,15–17].

Conventional TiO_2 photocatalysis suffers from low photonic efficiencies, which prevents application of photocatalytic technology for large scale water treatment operations [18]. Increasing the photonic efficiency and degradation rate constants of photocatalytic processes is an ongoing goal that is primarily focused on optimizing operational conditions such as catalyst type, catalyst concentration, light intensity, pH, and temperature [19]. A simple approach to increasing photonic efficiency is to optimize the light intensity or to use a doped catalyst [20–23] that increases light adsorption and/or lowers carrier recombination [23,24].

Light intensity is typically linearly proportional to the kinetic reaction rate constant at low intensities. At high light intensities, the square root of light intensity is proportional to the kinetic reaction rate constant [19,25,26]. The photonic efficiency is therefore limited at high light intensities. However Sczechowski et al. suggested that intermittently turning on and off a UV source, known as controlled

periodic illumination (CPI) can increase the photonic efficiency of TiO_2, while reducing light exposure times [27]. The practical application of CPI was limited with mercury lamps due to the warm up time required to output light and the tendency of filament failure if the lamp is turned on and off too quickly and frequently. Potential solutions, such as a rotating disk reactor with a pneumatic shutter [28], cannot be scaled up without substantially increasing economic and energetic costs. Additionally, the workable wavelength of undoped TiO_2 photocatalysis is below 400 nm and mercury lamps possess some emission peaks above the wavelength for undoped TiO_2 photocatalysis, limiting the energetic efficiency of these light sources. With the advent of UV-LED technology, it is possible to pulse UV-LEDs using microcontrollers and pulsed width modulation (PWM), increasing the lifespan of the light source and lowering energy expenditure [18]. UV-LEDs can utilize much of the light energy that is emitted because of its single, narrow Gaussian distribution [29–31]. The use of microcontrollers also allows for easy customizability and optimization of conditions such as frequency and duty cycle, which would not have been feasible with a traditional mercury lamp.

An analog of CPI employs the concept of Parrondo's paradox, the unexpected outcome in which two "losing" strategies can, by alternating them, produce a favourable outcome. Parrondo's paradox applied to photocatalytic processes may generate a higher yield of a measured product of interest when switching between UV light and dark conditions compared to the steady-state condition alone, even though the total irradiation period is lower than under steady-state illumination. Examples of this paradoxical behaviour under TiO_2 photocatalysis includes the study by Tada et al. which demonstrated that using Pt-shell/Ag-core particles loaded on TiO_2 and applying light on-off cycles to thiol (2-mercaptopyridine) the H_2 production rate was greater than steady-state illumination or dark adsorption, which produced no H_2 [32]. Additionally microorganisms and organic compounds under high frequency UV light on-off cycles showed higher removal compared to continuous illumination using similar UV intensities [33,34].

All of the current CPI studies observed photochemical reactions using a single pollutant source [18,28,33–36]. However, natural water matrices contain many pollutants and components that compete

for adsorption sites in photocatalysts, thereby affecting the kinetic rate constants of pollutant removal [8]. Understanding the CPI conditions in complex matrices is of interest because cycling conditions may influence interactions within this system that result in unexpected outcomes compared to single pollutant sources and under steady-state conditions [37].

This study investigates the removal rate constants of 18 pharmaceuticals and personal care products (PPCPs) using synthesized porous titanium – titanium dioxide (PTT) substrates under CPI conditions using UV-LEDs. PPCPs are emerging contaminants (ECs) that are of major concern in source waters and have been investigated in recent years due to their increase in concentration in wastewater treatment plant (WWTP) discharges from human activities, including urban activity and development and agriculture [13,38,39], [40,41]. The apparent kinetic rate constants from the removal of PPCPs were correlated to their net charge, molecular weight, and solubility. The UV-LED pulse profile was controlled by duty cycle at a constant pulse frequency to observe the decomposition of a pharmaceutical cocktail containing eighteen pharmaceuticals over time. The study also investigates the electric energy consumption of the CPI-controlled UV-LED/TiO_2 processes compared to steady-state conditions.

2. MATERIALS AND METHODS

2.1 Reagents and chemicals

All solvents and chemicals for synthesis methods were purchased from Sigma Aldrich at >99% purity. Ultrapure water (18.2 mΩ·cm resistivity at 25^{o}C) was obtained from a Milli-Q® Integral Water Purification System by EMD Millipore. The suppliers for all the reagents and chemicals for running experiments (parent compounds, metabolites, and deuterated standards), sample preparation, and LC-MS/MS analysis are described in previous work [8].

2.2 PTT substrate synthesis

The PTT substrate synthesis was similar to prior work [8,17]. Briefly, the porous titanium (PTi) sheets (0.254 mm thickness, Accumet Materials, Ossining, NY, USA) were cut into 50 mm diameter substrates and cleaned with ethanol and water. PTi substrates were immersed in 50 mL of 30% H_2O_2 in a jar (500 mL) at 80 ^{o}C for 2 h. After the reaction, oxidized PTi substrates were washed in water, dried at

80°C for 8 h, and calcined at 600°C for 2 h. The resultant substrates had an oxidized TiO_2 surface on porous titanium (PTT). It has previously been determined by Arlos et al. that the PTT substrates could be re-used without effecting the results [8]. The membranes were cleaned by heat treatment at 400°C for 3 h between uses to ensure there was not any carry-over between experiments.

2.3 Materials characterization

The morphology and features of PTi and PTT substrates was characterized using scanning electron microscopy (FE-SEM LEO 1550, Carl Zeiss Microscopy). Micro-Raman spectroscopy (Renishaw, He-Ne laser: λ = 632.8 nm) and X-ray diffraction (XRD, XPERT-PRO) were used to determine the crystal structure.

2.4 CPI UV-LED/TiO_2 setup and experimental methods

2.4.1 PPCPs and pharmaceutical metabolites

Eighteen PPCPs and metabolites were selected and analyzed for the experiments based on previous studies and their prevalence in the environment (see Table 1 for a list of the compounds and their characteristics) [8,17,42,43]. Stock solutions of PPCPs (1 g L^{-1}) in methanol were prepared and stored at -20°C when not in use and the appropriate amount was pipetted into the reaction mix when needed [8]. Methanol was used to dissolve all pharmaceuticals at some expense to the degradation performance on photocatalysis [8,17]. This is due to the methanol scavenging holes and hydroxyl radical species, which has been addressed for a similar combination of PPCPs and catalyst in a previous study [8]. Despite the well-established effect of methanol, it was still used to improve the solubility of the PPCPs. Care was taken to ensure the concentration of methanol was consistent between reactions, so that its effect would be consistent. The inclusion of a scavenger also better-mimics the complex matrices that are seen in wastewater treatment, which is a goal of this work.

2.4.2 UV-LED CPI standardized setup

The experimental setup consisted of a stir plate, collimated UV-LED column, and a microcontroller arranged as seen in Fig. 1. The UV-LED was controlled using a microcontroller (Arduino) coupled with a LED Current Driver (LEDSEEDUINO) and a pulsed-width modulation (PWM)

script was programmed into the controller (see Pulse Width Modulation Setup section in Supporting Information for details). The average power of the UV-LEDs was measured using a power and energy meter (Thorlabs, PM100-USB). The UV-LEDs provided 1.7 x 10^{-3} W of power at a wavelength of 365 nm. The power output of the UV intensity was measured from 10.5 cm from the UV-LED source is also shown in Table 2. The pH conditions (around pH ~ 5) were not adjusted.

The pharmaceutical stock solution was spiked into a beaker containing 300 mL of ultrapure water (2 µg L^{-1}). The methanol concentration of the spiked solution was 5 x 10^{-3} mM. The PTT substrates were placed on stainless steel holders inside the beakers with stir bars underneath. The beakers were placed on a digital magnetic stir plate (four-position, Talboys), three of which contain a UV-LED (λ= 365 nm) collimating column with a beam size of 4 cm. The UV-LEDs were situated 10.5 cm from the starting water level of the reactor with the PTT filter (sitting on the holder) 1.5 cm under the water level.

The PTT batch reactor was illuminated under steady and intermittent UV light regimes using five duty cycles at a constant pulse frequency of 1 Hz and two frequencies at a constant duty cycle of 50% with varying light and dark times (t_{on} and t_{off}) as described in Table 2. The cycle is defined as the period of illumination for a complete light and dark cycle and is the sum of the time on (t_{on}) and the time off (t_{off}-), whereas the duty cycle and frequency are defined as:

$$\gamma = \frac{t_{on}}{t_{on} + t_{off}} * 100\% \qquad \text{Eqn. 1}$$

$$f_{pulse} = \frac{1}{t_{on}+t_{off}}. \qquad \text{Eqn. 2}$$

2.4.3 Sample preparation and analysis

Sample preparation and analysis was similar to previous work by Arlos et al. [8,17]. Aliquoted samples (4 mL) were spiked with deuterated standard stock solution to a final concentration of 20 µg L^{-1}. Solid phase extraction (SPE) was not used as in previous publications because an ultrapure water matrix was used and no natural organic matter or other sources that could clog the liquid chromatography column were present [8,17]. Two 4 mL samples of ultrapure water were spiked with both 32 μL of 100

μg L^{-1} regular and deuterated standard solution. A negative control consisting of 4 mL of ultrapure water was added to serve as a blank. Samples were evaporated completely using a solvent evaporator (Dionex SE 500, Thermo Scientific, Mississauga, ON). The dried samples were reconstituted with 160 μL of methanol. The samples were transferred into 2 mL amber glass vials with plastic inserts, capped, and stored at -20^{o}C until analysis (less than two weeks).up to a week later.

The analysis of the compounds was completed using Agilent 1200 HPLC (Agilent Technologies) coupled to a mass spectrometer (3200 QTRAP, ABSciex, Concord, ON). The optimized parameter values, including chromatographic and ionization parameters, data acquisition, and quantitation are detailed in Tables S1-S3.

2.4.4 Multiple regression and correlation analysis

OriginLab (Version 8.0) was used to plot data and perform statistical analyses. Measured removal rate constants were fitted using pseudo first-order models. Multiple regression and correlation analyses were conducted on experimental sets. A multiple regression model was selected based on the relationship between the dependent variable, the kinetic rate constant, and three independent variables - net charge at experimental pH, molecular weight, and solubility - obtained from an online chemical database (Chemicalize, ChemAxon Ltd.). The best model was chosen based on minimizing the residual sum of squares, maximizing R^2, and testing for the significance of the variables. Correlation analysis was performed on the dependent and independent variables. Three correlation coefficients (Pearson's r, Spearman's ρ, Kendall's τ) that measure monotonic relationships were used. These correlation coefficients help discern whether the relationship is linear or non-linear (e.g. exponential, piecewise linear, and power functions). Spearman and Kendall's coefficients are resistant to the effect of outliers, whereas Pearson's r measures linear correlations, a specific type of monotonic relationship, and is affected by outliers [44].

3. RESULTS AND DISCUSSION

3.1 PTT Membrane characterization

TiO_2 was synthesized on porous titanium (PTi) substrates as shown in Fig. 2. The unprocessed PTi substrate has an average pore size of 10 μm using a thermal sintering process (Fig. 2a). The porosity of the substrate was 50% according to the manufacturer. Although the increase in porosity is proportional to the surface area and the number of adsorption sites will increase as a result, there is a trade-off to the mechanical strength of the substrate or adsorbent. When the porosity of absorbent exceeds 50%, it is more brittle and has lower mechanical strength [45]. The thermal-chemical oxidation of PTi occurred under 30% H_2O_2 and produced an oxidized TiO_2 surface containing a TiO_2 complex. Upon drying, the PTi-TiO_2 complex was heat treated at 600^{o}C to form porous titanium – titanium dioxide (PTT) substrate. The difference can be seen by comparing Fig. 2b and Fig. 2a. TiO_2 hierarchical nano-structures assembled on the surface of Fig. 2b were generated through the thermal oxidation process.

The material characterization methods and values for the PTT substrate are given in Table 3. The PTT substrates weigh 1.33 ± 0.08 g and have an average surface roughness determined to be 5-10 μm [17]. The Raman spectra indicate that the TiO_2 surface of the PTT substrate is of anatase phase (Fig. 3a). The PTi support showed no Raman peaks indicative of TiO_2 crystalline phases (Fig. 3a). XRD confirms that there are also rutile and titanium crystalline phases in the PTT sample along with the anatase phase (Fig. 3b). The bandgap energy of PTT was estimated to be at 3.0 eV derived from the Tauc plot in previous work [8], which corresponds to crystalline TiO_2. The isoelectric point was determined to be 6.0 based on previous work [8].

3.2 UV-LED/TiO_2 process against dark and photolysis controls

The normalized parent compound concentration was used to determine the total cumulative pharmaceutical removal after the 60 min equilibration period, which is defined as:

$$Normalized\ Parent\ Compound\ Concentration = \frac{\sum_1^i C_{i_t}}{\sum_1^i C_{i_0}} \qquad \text{Eqn. 3}$$

where i is the number of compounds tested, C_{i_t} is the concentration of the i^{th} compound at time t, and C_{i_0} is the initial concentration of the i^{th} compound. The photocatalytic degradation of the individual or

cumulative organic compounds can be modelled using Langmuir-Hinshelwood kinetics [46]. At low concentrations of adsorbates, the kinetic equation can be simplified to a pseudo-first order reaction equation:

$$-r = \frac{dC}{dt} = -k_{app}C \quad \text{Eqn. 4}$$

and rearranged to its integrated form:

$$\ln\left(\frac{C}{C_o}\right) = k_{app}t \quad \text{Eqn. 5}$$

where k_{app} (min^{-1}) is the apparent first-order reaction rate constant, C is the concentration at time t, and C_0 is the initial concentration. The apparent kinetic constant was obtained by taking the slope of the $ln(C/C_0)$ *vs.* t plot. Cumulative kinetic rate constants were calculated from the average of all compound concentrations at each time point. Both individual compound and total parent compound kinetic rate constants were obtained.

Under continuous illumination the magnitude of the pharmaceutical removal rate constant was 2.6 x 10^{-3} min^{-1}. The fastest-removed compound was o-ATOR, with a rate of -2.195 x 10^{-2} min. The average removal rate was lower compared to previous studies due to higher total pharmaceutical concentration and substrate compound adsorption selectivity [8,17]. The surface charge of PTT substrate is positive at the experimental pH. The low removal rate constant is attributed to surface charge effects of pharmaceuticals that do not easily adsorb on the surface of the PTT substrate, such as negatively charged compounds (venlafaxine, atenolol, norfluoxetine, and fluoxetine) [8]. The individual compound kinetic rate constants are found in Table S4 and confirm that anionic compounds were not removed. The cumulative pharmaceutical removal profile (Fig. 4) depicts the changes in concentration over the 300 minute UV exposure time. The continuous UV illumination of the PTT substrate shows a statistically significant removal compared to pure photolysis (p<0.04) and dark (p<0.004) conditions in which little to no reductions in concentrations were observed. There was no significant difference between dark and photolysis conditions (p>0.1).

3.3 Effect of net charge, molecular weight, and solubility on kinetics

The different decomposition rate constants of pharmaceuticals can be attributed to many physical and chemical characteristics of the PPCPs used in the study. The dark and photo-adsorption processes inherent in the TiO_2/UV advanced oxidation process are dictated by the summation of interactions and forces in three interfaces: the adsorbate-adsorbent, the adsorbate and water, and the water and adsorbent [45]. These forces cannot be readily measured. They can, however, be related to measurable parameters such as pH, net surface charge, solubility, and size [45]. Adsorption is also driven by pH as the pH affects both the charge of the PTT substrate which has an isoelectric point of 6.0, and the charge of ionizable polar species in PPCP compounds.

The different multiple regression models in Table 4 were used to relate the apparent kinetic rate degradation constant of PPCPs using TiO_2/UV under continuous illumination with three explanatory variables: net charge, molecular weight, and solubility. The 18 compounds are a mixture of PPCPs that are negatively charged (n = 8), neutral (n= 4), and positively charged (n = 6) at experimental pH. Additionally, the solubility of PPCPs range between 8 orders of magnitude. Regression analysis was first conducted on net charge alone (R^2 = 0.62), followed by the sequential addition of molecular weight (R^2 = 0.82) and solubility (R^2 = 0.89). Each added variable improved the model based on higher adjusted R^2 and lower residual sum of squares when compared to one or two explanatory variables alone. All of the independent variables inputted were significant using t-tests at $\alpha = 0.05$. The overall model using one-way ANOVA (Table S6) was also significant ($p < 0.000$).

Correlation analysis was used to measure relationships with the apparent kinetic rate constant, the dependent variable, and the three independent variables: net charge, molecular weight, and solubility. The kinetic rate constant was monotonically correlated with the net charge of pharmaceuticals. The experimental pH of this study was 5, which means that the PTT substrate had a net positive charge and would attract and preferentially adsorb ionisable PPCP species with a net negative charge. This behaviour was demonstrated by the removal of anionic compounds and lack of removal of cationic compounds as shown in Fig. 5a. The monotonic relationship between the kinetic rate constant and charge may not be

linearly correlated. Pearson's coefficient (r = -0.80) is sufficient to assume linearity, however Spearman's coefficient (ρ = -0.91) is higher than r, suggesting that the relationship is non-linear. A power law, also known as Pareto Principle or the 80/20 rule, may be feasible to model this relationship. The most negative pharmaceutical compounds at the experimental pH tend to degrade the fastest and represent much of the removal during the first 60 min under illumination, whereas less negative, neutral, and positive compounds are degraded much slower, or not at all. For instance, the five compounds with the highest negative net charge – diclofenac, atorvastatin, *o*-hydroxy atorvastatin, *p*-hydroxy atorvastatin, and naproxen – represent close to 22 % of the total pharmaceuticals in the water matrix tested, but account for 75.0 $\pm$ 3.3 % of the total compound removal after 60 min of illumination.

There is a weak, significant correlation between the apparent kinetic rate constant and solubility (p = 0.04), and a weak, non-significant relationship with molecular weight (p = 0.25) when all eighteen compounds are considered (see Fig. 5b and Fig. 5c). The correlation coefficients are stronger when compounds with negative net charge are considered. The relationship between the kinetic rate constants of negative compounds and molecular weight is monotonic and significant using Pearson's coefficient (r = -0.76, p = 0.030) and Spearman's coefficient (ρ = -0.80, p = 0.017). There is an even stronger monotonic relationship between the kinetic rate constant and solubility of negatively charged PPCPs using Pearson's coefficient (r = -0.75, p = 0.030) and Spearman's coefficient (ρ = 0.87, p = 0.005). Kendall's coefficient, τ, is usually smaller than both r and ρ but are above $|\tau|$ = 0.70, suggesting that there are good monotonic relationships between apparent kinetic rate constant and the independent variables of molecular weight and solubility.

3.3 The effect of duty cycle on the UV/TiO_2 process

To determine the effect of duty cycle on the apparent kinetic rate constants, duty cycles of γ = 0% (dark), 10%, 25%, 50%, 75%, and 100% (continuous) at a constant pulse frequency of 1 Hz were tested (results are shown in Fig. 6a and Table S4) and the significance was calculated using one-way ANOVA (Table S7A). At 0% (dark), there is little to no cumulative removal (k_{app} < 1x10^{-4} min^{-1}), which is significantly different compared to all duty cycles tested (p<0.001). This indicates that dark adsorption

has no effect after the initial 60 min equilibrium time. There are also no significant differences in cumulative removal between any two γ above 0 % at the α = 0.05 significance level (see Table S7A). However, there was a significant difference in the kinetic rate constant at γ = 25 % compared to γ = 100 % and at γ = 25 % compared to γ = 10 % at the α = 0.05 significance level. Overall changing the duty cycle from a range between 10 % to 100 % has no bearing on the overall apparent kinetic rate constant. Further, it became apparent that the photocatalytic reaction of the PPCP cocktail on the PTT substrate is much more efficient under longer t_{off} periods. It is therefore concluded that the reaction is not photon-limited.

In a study by Xiong and Hu [33], CPI-controlled UV/TiO_2 was used to decompose acetaminophen at relevant treatment concentrations in the parts per billion range. The kinetic rate constant results were adjusted by normalizing with the kinetic rate constant at γ = 100% and plotted as a function of duty cycle. The results were compared to the results in this work in Fig. 6b. Both experiments were conducted at a similar pH and light intensity, however in Xiong and Hu's experiment the pulse frequency time is an order of magnitude higher and a TiO_2 slurry was used rather than an immobilized TiO_2 substrate. Their results showed that the kinetic rate constant value decreases linearly as γ decreases from 20% to 80% even though the photonic efficiency increases. In the current work, there was no significant difference in the kinetic rate constants between the lowest duty cycle tested (γ = 10%) and continuous irradiation (γ = 100%). In the case of Xiong and Hu, the decrease in kinetic rate constants when decreasing γ was due to less photon generation because the dark time, t_{off}, increases and would be considered a rate-limiting step. In our work mass transfer was the rate-limiting step due to three possible factors: the lack of adsorption of positively charged and neutral pharmaceuticals, the relative difficulty in transferring micropollutants to a substrate compared to a slurry batch reactor, and less adsorption sites in TiO_2 substrate compared to a TiO_2 particle-based slurry batch reactor [25]. Under a mass-transfer limited regime the dependency of the reaction rate constant to light intensity is negligible (0^{th} order) because of

saturated surface sites, low adsorption/desorption rates, and desorption products that may promote recombination [25].

Only negatively charged compounds and select neutral compounds showed removal by photocatalysis with all γ tested, including continuous illumination (γ = 100%). Lowering the duty cycle from 100% did not affect removal characteristics. The most negatively charged compounds still degraded first, select neutral compounds showed low removal rate constants, and positively charged compounds showed no removal. Fig. 7a depicts the negatively charged compounds that were capable of being removed at all duty cycles from 10% to 100% above the threshold of $|k_{app}| = 0.1x10^{-2}$ min^{-1}. All other compounds did not show removal above the threshold, except neutral compounds such as TCS and TCCB (Fig. 7b). There was no significant difference in removal rate constants between γ for any individual compound, which matches the results obtained from the cumulative pharmaceutical removal rate constants at α = 0.05 (Table S7B).

3.4 The effect of pulse frequency on the UV/TiO_2 process

The effect of pulse frequency was determined under three pulse frequency profiles: 0.05 Hz, 25 Hz, and alternating between 25Hz for 500 cycles and 1 cycle at 0.05 Hz (dual frequency) at γ = 50% (Fig. 8). There were significantly different removal rate constants using one-way ANOVA (Table S8A) under continuous irradiation compared to 0.05 Hz pulse profile (p = 0.014) and dual frequency compared to the 0.05 Hz profile (p = 0.002). There is also a significant difference between the 0.05Hz profile and the 25 Hz profile (p = 0.025). All other comparisons were not significant at the α = 0.05 significance level.

Under the dual frequency profile, the total pharmaceutical parent compound kinetic rate constant was greater than the 25 Hz and 0.05 Hz profiles alone (Fig. 9). This suggests that switching between high frequency and low frequency profiles can generate higher kinetic removal rate constants due to interactions between pharmaceuticals and the PTT substrate in the water matrix. There are no statistical differences between the 25 Hz and 0.05 Hz frequency profiles of individual compounds (Table S8B). However under 0.05 Hz the average kinetic rate constants of more negatively charged compounds were

higher than under the 25 Hz profile but lower with more neutral compounds. The dual frequency profile has a synergetic effect that takes advantage of both single frequency profiles and has higher average degradation rate constants than individual 0.05 Hz and 25 Hz profiles. One compound, gemfibrozil, had a higher average kinetic rate constant under the dual frequency regime than at 0.05 Hz (p = 0.021, α = 0.05) and at 25 Hz (p = 0.096, α = 0.10). The difference between continuous and dual frequencies is not significant, even though the kinetic rate constant is slightly higher compared to dual frequency than in the continuous regime k_{app}=-(2.39 $\pm$ 0.36) x 10^{-3} min^{-1}.

3.5 Implications and energy analysis of the CPI controlled TiO_2/UV process

The photocatalytic process is initiated by UV light when the irradiation energy is greater than the TiO_2 band gap energy. The generation of electrons and holes is in the order of femtoseconds. Slower reaction processes that do not require UV illumination and occur at the nanosecond to millisecond range are rate-limiting steps for TiO_2 photocatalysis [18,47]. These slower reaction processes include charge-carrier trapping, recombination, and interfacial charge transfer [18]. The incident photons that initiate charge separation are not efficiently used due to charge carrier recombination, which occurs from 0.1 ns (shallow trap states) to 10 ns (deep trap states). Recombination is faster than the interfacial charge transfer processes, so it limits charge transfer processes that are necessary for redox reactions [18,35]. Sczechowski et al. proposed that under continuous illumination, photocatalytic reactions will build-up electron-hole (e^-/h^+) charges and photogenerated species ($OH^*/O_2{}^{*-}$), leading to undesirable reactions that lower the photonic efficiency [27,48]. The introduction of CPI and alternating the t_{on} and t_{off} UV-LED profiles can limit these undesirable reactions.

Ku et al. modelled the interfacial charge transfer processes under CPI by establishing transient and steady-state balances of holes and electrons, then generating a surface coverage profile for the adsorbate, dimethyl phthalate (DMP), OH^-, O_2, and $O_2{}^{*-}$. It was assumed that DMP molecules were adsorbed onto the TiO_2 surface, while electron-hole pairs were generated during the illumination period. DMP was oxidized into smaller constituents by radical species generated from interfacial charge transfer

(OH*, O_2^{*-}, and h^+) and were then desorbed from the TiO_2 surface. During the dark period adsorption and desorption of reacting species and products occur as they do under illumination. The model showed that the carrier recombination of photo-induced electrons and holes was enhanced with decreasing surface coverage of OH^- or DMP due to charge build-up when the illumination time was increased. The dark period allows $O_2^{\bullet-}$ to react with DMP, which may increase the surface coverage due to desorption oxidation of DMP molecules [35]. Once the surface coverage is replenished DMP, OH-, and O_2 molecules can be adsorbed under illumination. The overall process improves the utilization efficiency of photons.

Because of the increased efficiency in the utilization of photons with CPI, it is expected that energy consumption for photocatalytic systems can be improved through periodic illumination. The evaluation of the unit treatment costs is one aspect that requires attention. Since the UV/TIO_2 process requires electrical energy and can represent a significant amount of operating cost when it is scaled, figures-of-merit based on electrical energy consumption may be informative. Electrical energy per order removal (E_{EO}, Wh m^{-3} $order^{-1}$) for low pollutant concentrations was determined for a batch-type reactor using the following equation [35,49]:

$$E_{EO} = \frac{38.4 P_{el}}{V \times k_{app}} \qquad \text{Eqn. 6}$$

Where P_{el} is the input power (W) to the UV-LED system, V is the volume of water (L) in the reactor, and k_{app} (min^{-1}) is the apparent rate constant.

In Fig. 10a the E_{EO} of the UV-LED source increases linearly with increasing illumination time (duty cycle) at a constant irradiation pulse frequency of 1 Hz. Under the same experimental time of 5 h, the electric energy per order was decreased by a factor of ten from τ=100% to τ=10%. The decrease in energy required to remove an order of magnitude of pollutants is much lower using CPI at low τ for the PTT substrate and may represent significant cost savings in energy if implemented in a larger scale for photocatalytic operations. Similarly the implementation of alternating single frequency profiles (dual

frequency) also lowers energy consumption compared to single frequency profiles alone without changing the duty cycle. The dual frequency profile lowers the E_{E0} by around 35 to 45% compared to continuous illumination.

4. CONCLUSIONS

UV-LED/TiO_2 photocatalytic decomposition of PPCPs was first conducted under continuous UV conditions. The kinetic rate constants of decomposition were affected by the water matrix containing 18 pharmaceuticals of varying net charge, solubility, and molecular weight. The net charge at the experimental pH was the main factor in determining the kinetic rate constant of the decomposition of a specific PPCP compound, in which negatively charged compounds degrade first and positive compounds do not degrade over the time span of the experiment. Other factors such as solubility and molecular weight also explain the variations in kinetic rate constants using a multiple regression model.

Programming UV-LEDs to operate under CPI and applying the process in TiO_2 photocatalysis was determined to be an effective treatment option when TiO_2 is immobilized on a substrate. The electrical energy that is required to reduce the concentration per order of magnitude, E_{E0}, is lower at lower duty cycles (τ <50%) than under continuous illumination. These results occur because mass-transfer is the rate-limiting step, so there was no significant difference between using τ=10% and τ=100%. Additionally, τ=10% requires a tenth of the light source energy required to reduce the concentration of the PPCP compound mixture by an order of magnitude compared to τ=100%. Alternating frequency profiles also lowered the E_{E0} compared to continuous illumination without changing the duty cycle. Under a mass-transfer limited regime, the dependency of the reaction rate constant to light intensity is negligible. This could be mitigated by using TiO_2 particle based suspensions and increasing fluid turbulence, which would increase the energy costs of operation, including particle separation steps. CPI is a feasible method from an operational standpoint to lower energy costs of light sources using immobilized TiO_2. Using CPI UV/TiO_2 process with complex water matrices, containing microorganisms or natural organic matter, may

be studied in the future to understand its effects and whether there are varying treatment outcomes compared to continuous illumination.

ACKNOWLEDGEMENTS

This work was funded through the Natural Sciences and Engineering Research Council (NSERC) of Canada – Strategic Project Grant (STPGP 430654-12). We would also like to acknowledge the help and assistance provided by the Schwartz-Resiman Foundation under the Waterloo-Technion Research Co-operation Program.

REFERENCES

[1] R.T. Williams, ed., Human Pharmaceuticals: Assessing the Impacts on Aquatic Ecosystems, SETAC Press, Pensacola, FL, 2005.

[2] K. Natarajan, T.S. Natarajan, H.C. Bajaj, R.J. Tayade, Photocatalytic reactor based on UV-LED/TiO 2 coated quartz tube for degradation of dyes, Chem. Eng. J. 178 (2011) 40–49. doi:10.1016/j.cej.2011.10.007.

[3] T.S. Natarajan, M. Thomas, K. Natarajan, H.C. Bajaj, R.J. Tayade, Study on UV-LED/TiO 2 process for degradation of Rhodamine B dye, Chem. Eng. J. 169 (2011) 126–134. doi:10.1016/j.cej.2011.02.066.

[4] A. Vázquez, D.B. Hernández-Uresti, S. Obregón, Electrophoretic deposition of CdS coatings and their photocatalytic activities in the degradation of tetracycline antibiotic, Appl. Surf. Sci. 386 (2016) 412–417. doi:10.1016/j.apsusc.2016.06.034.

[5] Q. Chen, Y. Xin, X. Zhu, Au-Pd nanoparticles-decorated TiO 2 nanobelts for photocatalytic degradation of antibiotic levofloxacin in aqueous solution, Electrochim. Acta. 186 (2015) 34–42. doi:10.1016/j.electacta.2015.10.095.

[6] K. Mitamura, H. Narukawa, T. Mizuguchu, K. Shimada, Degradation of Estrogen Conjugates Using Titanium Dioxide as a Photocatalyst, Anal. Sci. 20 (2004) 3–4. https://www.jstage.jst.go.jp/article/analsci/20/1/20_1_3/_pdf/-char/en (accessed September 19, 2018).

[7] R. Liang, A. Hu, W. Li, Y.N. Zhou, Enhanced degradation of persistent pharmaceuticals found in wastewater treatment effluents using TiO2 nanobelt photocatalysts, J. Nanoparticle Res. 15 (2013) 1990. doi:10.1007/s11051-013-1990-x.

[8] M.J. Arlos, M.M. Hatat-Fraile, R. Liang, L.M. Bragg, N.Y. Zhou, S.A. Andrews, M.R. Servos, Photocatalytic decomposition of organic micropollutants using immobilized TiO 2 having different isoelectric points, Water Res. 101 (2016) 351–361. doi:10.1016/j.watres.2016.05.073.

[9] R. Liang, M. Hatat-Fraile, H. He, M. Arlos, M.R. Servos, Y.N. Zhou, TiO 2 membranes for

concurrent photocatalytic organic degradation and corrosion protection, in: S. Cabrini, G. Lérondel, A.M. Schwartzberg, T. Mokari (Eds.), SPIE Nanosci. + Eng., International Society for Optics and Photonics, 2015: p. 95450M. doi:10.1117/12.2188466.

[10] M. Klavarioti, D. Mantzavinos, D. Kassinos, Removal of residual pharmaceuticals from aqueous systems by advanced oxidation processes., Environ. Int. 35 (2009) 402–17. doi:10.1016/j.envint.2008.07.009.

[11] J.M. Poyatos, M.M. Muñio, M.C. Almecija, J.C. Torres, E. Hontoria, F. Osorio, Advanced Oxidation Processes for Wastewater Treatment: State of the Art, Water. Air. Soil Pollut. 205 (2010) 187–204. doi:10.1007/s11270-009-0065-1.

[12] R.L. Fernández, J.A. McDonald, S.J. Khan, P. Le-Clech, Removal of pharmaceuticals and endocrine disrupting chemicals by a submerged membrane photocatalysis reactor (MPR), Sep. Purif. Technol. 127 (2014) 131–139. doi:10.1016/j.seppur.2014.02.031.

[13] R. Rosal, A. Rodríguez, J.A. Perdigón-Melón, A. Petre, E. García-Calvo, M.J. Gómez, A. Agüera, A.R. Fernández-Alba, Occurrence of emerging pollutants in urban wastewater and their removal through biological treatment followed by ozonation, Water Res. 44 (2010) 578–588. doi:10.1016/j.watres.2009.07.004.

[14] S. Esplugas, D.M. Bila, L.G.T. Krause, M. Dezotti, Ozonation and advanced oxidation technologies to remove endocrine disrupting chemicals (EDCs) and pharmaceuticals and personal care products (PPCPs) in water effluents, J. Hazard. Mater. 149 (2007) 631–642. doi:10.1016/j.jhazmat.2007.07.073.

[15] L. Rizzo, S. Meric, M. Guida, D. Kassinos, V. Belgiorno, Heterogenous photocatalytic degradation kinetics and detoxification of an urban wastewater treatment plant effluent contaminated with pharmaceuticals, Water Res. 43 (2009) 4070–4078. doi:10.1016/j.watres.2009.06.046.

[16] C. Martínez, M. Canle L., M.I. Fernández, J.A. Santaballa, J. Faria, Aqueous degradation of diclofenac by heterogeneous photocatalysis using nanostructured materials, Appl. Catal. B

Environ. 107 (2011) 110–118. doi:10.1016/j.apcatb.2011.07.003.

[17] M.J. Arlos, R. Liang, M.M. Hatat-Fraile, L.M. Bragg, N.Y. Zhou, M.R. Servos, S.A. Andrews, Photocatalytic decomposition of selected estrogens and their estrogenic activity by UV-LED irradiated TiO 2 immobilized on porous titanium sheets via thermal-chemical oxidation, J. Hazard. Mater. 318 (2016) 541–550. doi:10.1016/j.jhazmat.2016.07.048.

[18] O. Tokode, R. Prabhu, L.A. Lawton, P.K.J. Robertson, Controlled periodic illumination in semiconductor photocatalysis, J. Photochem. Photobiol. A Chem. 319–320 (2016) 96–106. doi:10.1016/j.jphotochem.2015.12.002.

[19] J.M. Herrmann, Photocatalysis fundamentals revisited to avoid several misconceptions, Appl. Catal. B Environ. 99 (2010) 461–468. doi:10.1016/j.apcatb.2010.05.012.

[20] W. Ho, J.C. Yu, S. Lee, Low-temperature hydrothermal synthesis of S-doped TiO2 with visible light photocatalytic activity, J. Solid State Chem. 179 (2006) 1171–1176. doi:10.1016/j.jssc.2006.01.009.

[21] R. Azouani, A. Michau, K. Hassouni, K. Chhor, J.-F. Bocquet, J.-L. Vignes, A. Kanaev, Elaboration of pure and doped TiO2 nanoparticles in sol–gel reactor with turbulent micromixing: Application to nanocoatings and photocatalysis, Chem. Eng. Res. Des. 88 (2010) 1123–1130. doi:10.1016/j.cherd.2009.10.001.

[22] Z. Xiong, X.S. Zhao, Nitrogen-doped titanate-anatase core-shell nanobelts with exposed {101} anatase facets and enhanced visible light photocatalytic activity., J. Am. Chem. Soc. 134 (2012) 5754–7. doi:10.1021/ja300730c.

[23] M. Pelaez, N.T. Nolan, S.C. Pillai, M.K. Seery, P. Falaras, A.G. Kontos, P.S.M. Dunlop, J.W.J. Hamilton, J.A. Byrne, K. O'Shea, M.H. Entezari, D.D. Dionysiou, A review on the visible light active titanium dioxide photocatalysts for environmental applications, Appl. Catal. B Environ. 125 (2012) 331–349. doi:10.1016/j.apcatb.2012.05.036.

[24] R. Asahi, T. Morikawa, T. Ohwaki, K. Aoki, Y. Taga, Visible-Light Photocatalysis in Nitrogen-Doped Titanium Oxides, Science (80-.). 293 (2001).

[25] M.N. Chong, B. Jin, C.W.K. Chow, C. Saint, Recent developments in photocatalytic water treatment technology: a review., Water Res. 44 (2010) 2997–3027. doi:10.1016/j.watres.2010.02.039.

[26] S. Malato, P. Fernández-Ibáñez, M.I. Maldonado, J. Blanco, W. Gernjak, Decontamination and disinfection of water by solar photocatalysis: Recent overview and trends, Catal. Today. 147 (2009) 1–59. doi:10.1016/j.cattod.2009.06.018.

[27] J.G. Sczechowski, C.A. Koval, R.D. Noble, Evidence of critical illumination and dark recovery times for increasing the photoefficiency of aqueous heterogeneous photocatalysis, J. Photochem. Photobiol. A Chem. 74 (1993) 273–278. doi:10.1016/1010-6030(93)80126-T.

[28] K.J. Buechler, C.H. Nam, T.M. Zawistowski, Design and Evaluation of a Novel-Controlled Periodic Illumination Reactor To Study Photocatalysis, Ind. Eng. Chem. Res. 38 (1999) 1258–1263. doi:10.1021/ie9806139.

[29] S. Vilhunen, H. Särkkä, M. Sillanpää, Ultraviolet light-emitting diodes in water disinfection, Environ. Sci. Pollut. Res. 16 (2009) 439–442. doi:10.1007/s11356-009-0103-y.

[30] K. Song, M. Mohseni, F. Taghipour, Application of ultraviolet light-emitting diodes (UV-LEDs) for water disinfection: A review, Water Res. 94 (2016) 341–349. doi:10.1016/j.watres.2016.03.003.

[31] M.A. Würtele, T. Kolbe, M. Lipsz, A. Külberg, M. Weyers, M. Kneissl, M. Jekel, Application of GaN-based ultraviolet-C light emitting diodes – UV LEDs – for water disinfection, Water Res. 45 (2011) 1481–1489. doi:10.1016/j.watres.2010.11.015.

[32] *,† Hiroaki Tada, ‡ Fumiaki Suzuki, ‡ Seishiro Ito, § Tomoki Akita, § Koji Tanaka, ∥ and Tetsuro Kawahara, H. Kobayashi⊥, Au-Core/Pt-Shell Bimetallic Cluster-Loaded TiO2. 1. Adsorption of Organosulfur Compound, (2002). doi:10.1021/JP0202690.

[33] P. Xiong, J. Hu, Decomposition of acetaminophen (Ace) using TiO2/UVA/LED system, Catal. Today. 282 (2017) 48–56. doi:10.1016/j.cattod.2016.03.015.

[34] E. Korovin, D. Selishchev, A. Besov, D. Kozlov, UV-LED TiO2 photocatalytic oxidation of

acetone vapor: Effect of high frequency controlled periodic illumination, Appl. Catal. B Environ. 163 (2015) 143–149. doi:10.1016/j.apcatb.2014.07.034.

[35] Y. Ku, S.J. Shiu, H.C. Wu, Decomposition of dimethyl phthalate in aqueous solution by UV–LED/TiO2 process under periodic illumination, J. Photochem. Photobiol. A Chem. 332 (2017) 299–305. doi:10.1016/j.jphotochem.2016.09.011.

[36] H.-W. Chen, Y. Ku, A. Irawan, Photodecomposition of o-cresol by UV-LED/TiO2 process with controlled periodic illumination., Chemosphere. 69 (2007) 184–90. doi:10.1016/j.chemosphere.2007.04.051.

[37] D.C. Osipovitch, C. Barratt, P.M. Schwartz, R.F. Ludlow, S. Otto, M. Kindermann, I. Stahl, M. Reimold, W.M. Pankau, G. von Kiedrowski, P. Compain, V. Desvergnes, C. Ollivier, F. Robert, F. Suzenet, M. Barboiu, P. Belmont, Y. Blériot, F. Bolze, S. Bouquillon, E. Bourguet, B. Braida, T. Constantieux, L. Désaubry, D. Dupont, S. Gastaldi, F. Jérome, S. Legoupy, X. Marat, M. Migaud, N. Moitessier, S. Papot, F. Peri, M. Petit, S. Py, E. Schulz, I. Tranoy-Opalinski, B. Vauzeilles, P. Vayron, L. Vergnes, S. Vidal, S. Wilmouth, G.P. Harmer, D. Abbott, G.P. Harmer, D. Abbott, A.P. Flitney, D. Abbott, J.M.R. Parrondo, G.P. Harmer, D. Abbott, J.M.R. Parrondo, L. Dinis, H. Martin, H.C. von Baeyer, W. Vance, J. Ross, M. Tsuchiya, J. Ross, R.D. Astumian, B. Robertson, R.S. Li, J. Ross, C. Antoine, A. Lemarchand, S.J. Broadwater, S.L. Roth, K.E. Price, M. Kobaslija, D.T. McQuade, C. Viedma, T.G. Park., A.S. Hoffman, T.G. Park, A.S. Hoffman, M.F. Kramer, D.M. Coen, H.A. Hansen, J.L. Olsen, S. Jensen, O. Hansen, U.J. Quaade, J.J. Brandner, G. Emig, M.A. Liauw, K. Schubert, S. Jensen, J.L. Olsen, S. Thorsteinsson, O. Hansen, U.J. Quaade, Systems chemistry and Parrondo's paradox: computational models of thermal cycling, New J. Chem. 33 (2009) 2022. doi:10.1039/b900288j.

[38] K. Noguera-Oviedo, D.S. Aga, Lessons learned from more than two decades of research on emerging contaminants in the environment, J. Hazard. Mater. 316 (2016) 242–251. doi:10.1016/j.jhazmat.2016.04.058.

[39] P.A. Bahamonde, M.L. Fuzzen, C.J. Bennett, G.R. Tetreault, M.E. McMaster, M.R. Servos, C.J.

Martyniuk, K.R. Munkittrick, Whole organism responses and intersex severity in rainbow darter (Etheostoma caeruleum) following exposures to municipal wastewater in the Grand River basin, ON, Canada. Part A, Aquat. Toxicol. 159 (2015) 290–301. doi:10.1016/j.aquatox.2014.11.023.

[40] J. Lu, J. Wu, P.J. Stoffella, P.C. Wilson, Uptake and distribution of bisphenol A and nonylphenol in vegetable crops irrigated with reclaimed water, J. Hazard. Mater. 283 (2015) 865–870. doi:10.1016/j.jhazmat.2014.10.018.

[41] V.S. Thomaidi, A.S. Stasinakis, V.L. Borova, N.S. Thomaidis, Is there a risk for the aquatic environment due to the existence of emerging organic contaminants in treated domestic wastewater? Greece as a case-study, J. Hazard. Mater. 283 (2015) 740–747. doi:10.1016/j.jhazmat.2014.10.023.

[42] A. Tong, TiO2-assisted photodegradation of pharmaceuticals — a review, Cent. Eur. J. Chem. 10 (2012).

[43] S. Kleywegt, V. Pileggi, P. Yang, C. Hao, X. Zhao, C. Rocks, S. Thach, P. Cheung, B. Whitehead, Pharmaceuticals, hormones and bisphenol A in untreated source and finished drinking water in Ontario, Canada — Occurrence and treatment efficiency, Sci. Total Environ. 409 (2011) 1481–1488. doi:10.1016/j.scitotenv.2011.01.010.

[44] D.R. Helsel, R.M. Hirsch, Statistical Methods in Water Resources, (n.d.).

[45] J.C. Crittenden, R.R. Trussell, D.W. Hand, K.J. Howe, G. Tchobanoglous, Adsorption, in: MWH's Water Treat., John Wiley & Sons, Inc., Hoboken, NJ, USA, 2012: pp. 1117–1262. doi:10.1002/9781118131473.ch15.

[46] C.S. Turchi, D.F. Ollis, Photocatalytic degradation of organic water contaminants: Mechanisms involving hydroxyl radical attack, J. Catal. 122 (1990) 178–192. doi:10.1016/0021-9517(90)90269-P.

[47] R. Memming, Photoinduced charge transfer processes at semiconductor electrodes and particles, Top. Curr. Chem. 169 (1994) 105–181.

[48] J.G. Sczechowski, C.A. Koval, R.D. Noble, A Taylor vortex reactor for heterogeneous

photocatalysis, Chem. Eng. Sci. 50 (1995) 3163–3173. doi:10.1016/0009-2509(95)00176-6.

[49] M. a Behnajady, B. Vahid, N. Modirshahla, M. Shokri, Evaluation of electrical energy per order (E EO) with kinetic modeling on the removal of Malachite Green by US / UV / H 2 O 2 process, Des. 249 (2009) 99–103. doi:10.1016/j.desal.2008.07.025.

FIGURE CAPTIONS

Figure 1: Experimental photocatalytic batch reactor with pulse width modulation (PWM) control unit containing a (a) microcontroller, (b) LED driver, and (c) UV-LED.

Figure 2: SEM images of (a) PTi substrate and (b) PTT substrate at low magnification (1) and high magnification (2).

Figure 3: (a) Raman and (b) XRD spectra of PTT substrates.

Figure 4: Cumulative pharmaceutical removal profile under dark and UV illumination conditions (with PTT substrate) and under photolysis (without PTT substrate).

Figure 5: Multiple regression analysis of kinetic rate constant as a function of (a) net charge, (b)molecular weight, and (c) solubility at experimental pH (pH=5). Negative (red), neutral (blue), and positive (green) compounds at experimental pH were distinguished. Highlighted region (light blue) represents region of interest for negative compounds only.

Figure 6: (a) Cumulative kinetic rate constants of PPCPs at various duty cycles at a pulse frequency of 1 Hz and (b) a comparison of normalized kinetic rate constants. Our work: $[Total_{PPCP}]$ = 42 ppb, PTT substrate, light intensity = 2.2 mW cm^{-2}, pH=5, pulse frequency = 1 Hz. Xiong and Hu: $[Ace]_0$=200 ppb, $[TiO_2]$=10 ppm, light intensity = 5.0 mW cm^{-2}, pH=5.6, pulse frequency = 10 Hz.

Figure 7: Kinetic rate constant of (a) negative, (b) neutral, and (c) positive compounds at various duty cycles.

Figure 8: The (a) Concentration vs. Time Profile and (b) Kinetic Rate Constants of total compound degradation at different frequencies (0.05 Hz, 25 Hz, Dual Frequency., and Continuous). Bars that do not share a common letter are significantly different at α = 0.05 significance level as determined by one-way ANOVA using the Tukey post-hoc test.

Figure 9: Kinetic rate constant of (a) negative, (b) neutral, and (c) positive compounds at different frequencies (0.05 Hz, 25 Hz, Dual Frequency, and Continuous).

Figure 10: Energy per order magnitude of UV-LED/TiO_2 process under various (a) duty cycles and (b) frequencies.

TABLE CAPTIONS

Table 1: Physical and chemical properties of target compounds

Table 2: Light profiles for dark, continuous, and periodic illumination under various duty cycles (γ).

Table 3: Material characteristics of PTT substrate.

Table 4: Multiple regression analysis (forward approach).

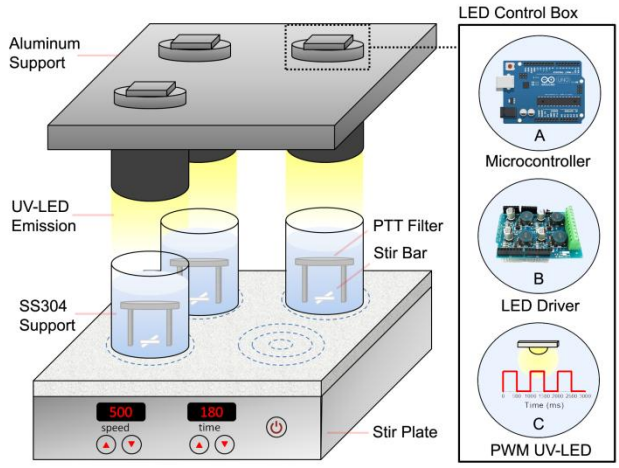

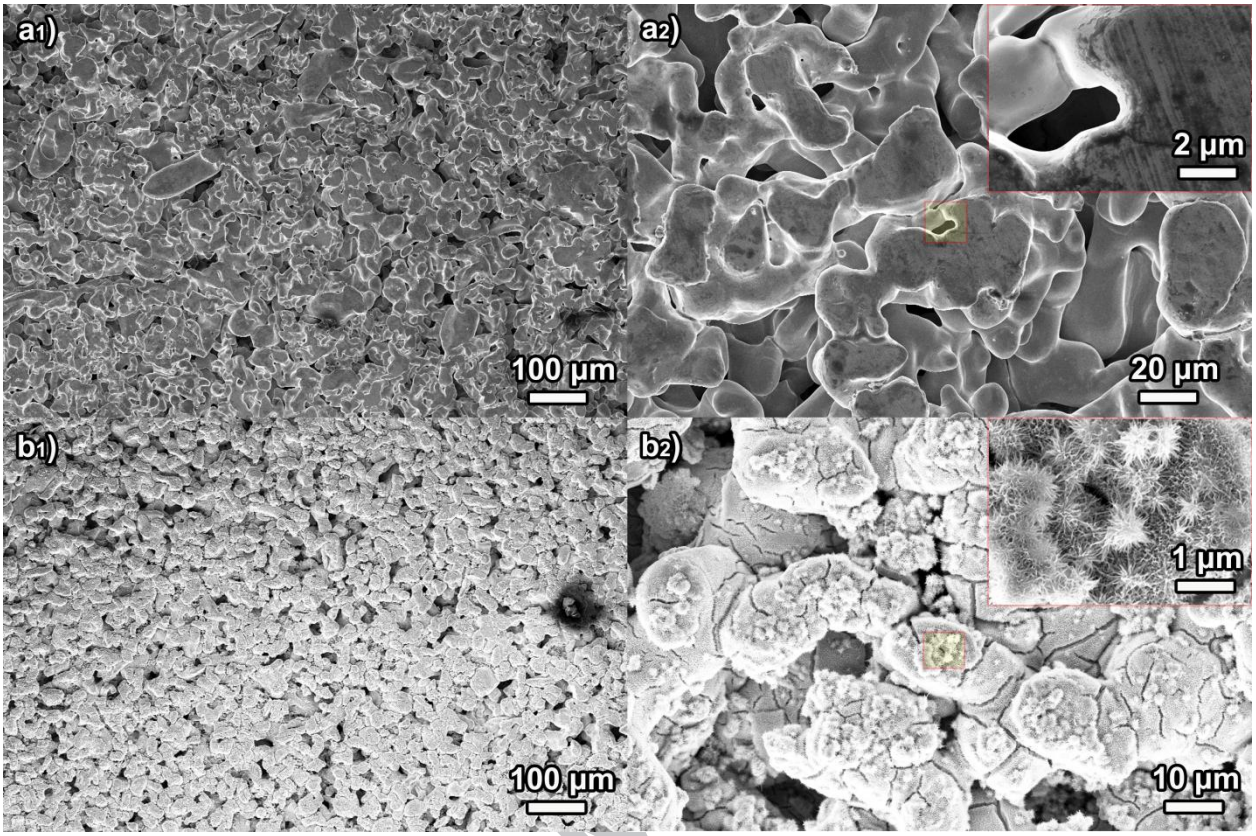

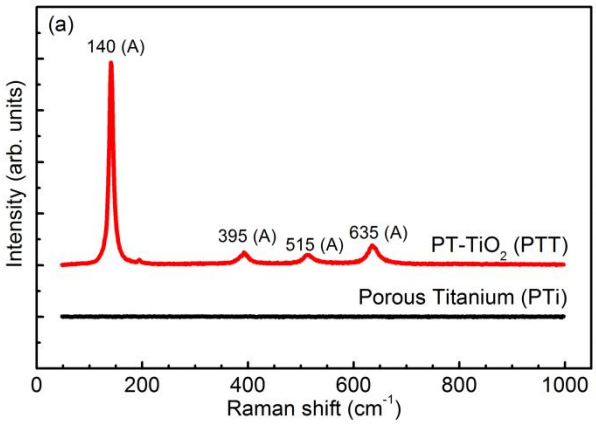

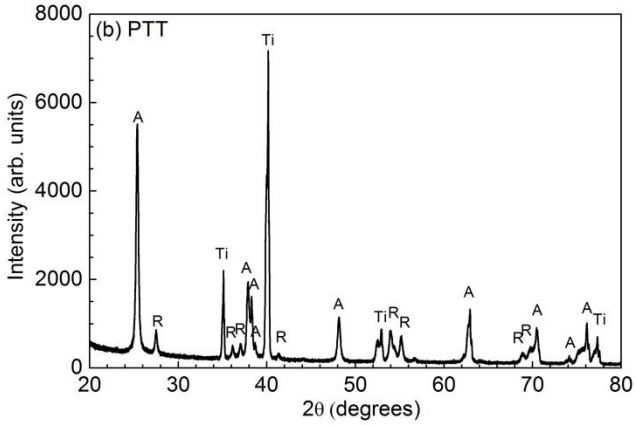

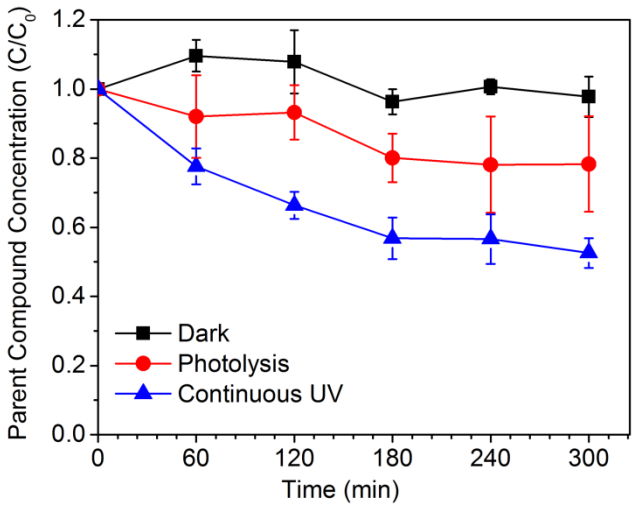

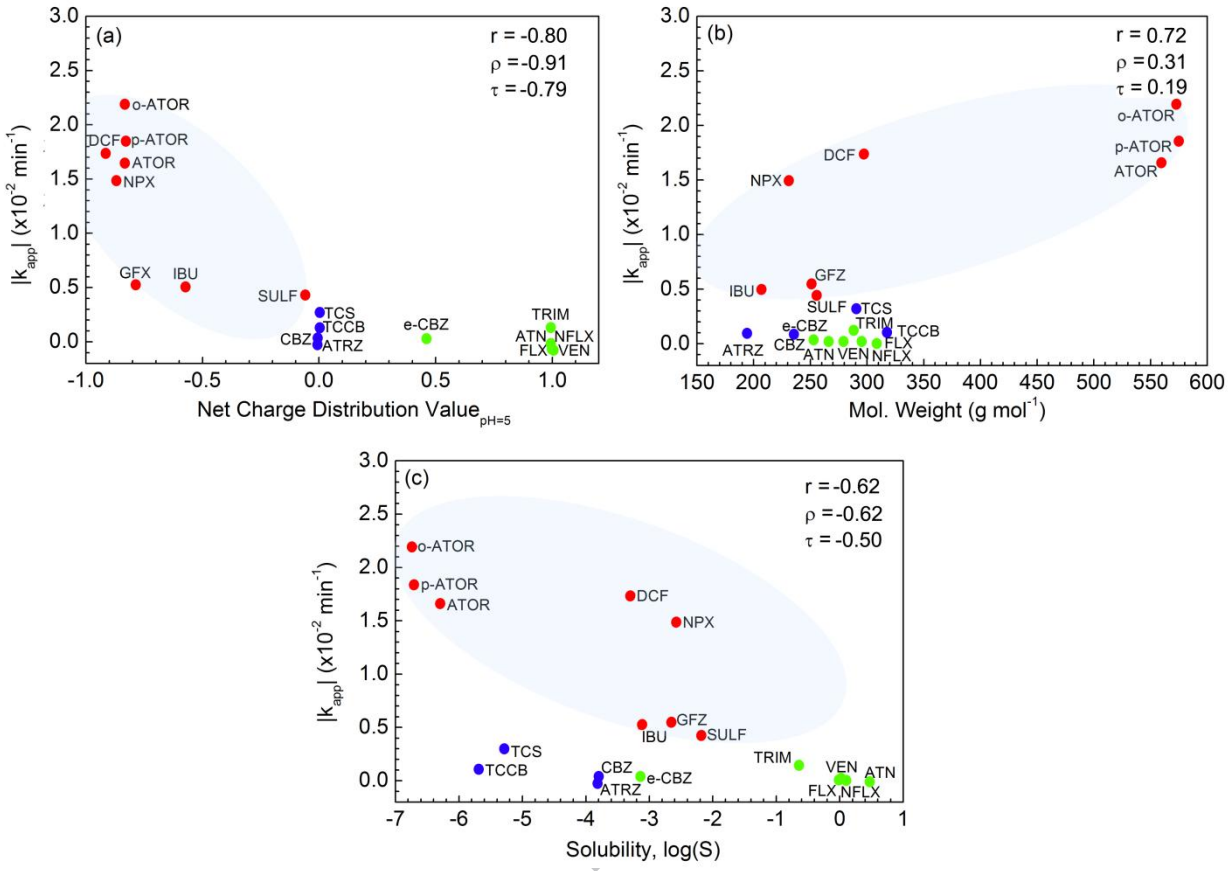
(a)
r = -0.80
ρ = -0.91
τ = -0.79
o-ATOR
DCF
p-ATOR
ATOR
NPX
GFX
IBU
SULF
TCS
TCCB
CBZ
ATRZ
e-CBZ
TRIM
ATN
NFLX
FLX
VEN
|k_app| (x10^-2 min^-1)
Net Charge Distribution Value_pH=5
(b)
r = 0.72
ρ = 0.31
τ = 0.19
o-ATOR
p-ATOR
ATOR
DCF
NPX
GFZ
IBU
SULF
TCS
TRIM
e-CBZ
TCCB
ATRZ
CBZ
ATN
VEN
NFLX
FLX
|k_app| (x10^-2 min^-1)
Mol. Weight (g mol^-1)
(c)
r = -0.62
ρ = -0.62
τ = -0.50
o-ATOR
p-ATOR
ATOR
DCF
NPX
GFZ
IBU
SULF
TCS
TCCB
CBZ
ATRZ
e-CBZ
TRIM
VEN
ATN
FLX
NFLX
|k_app| (x10^-2 min^-1)
Solubility, log(S)

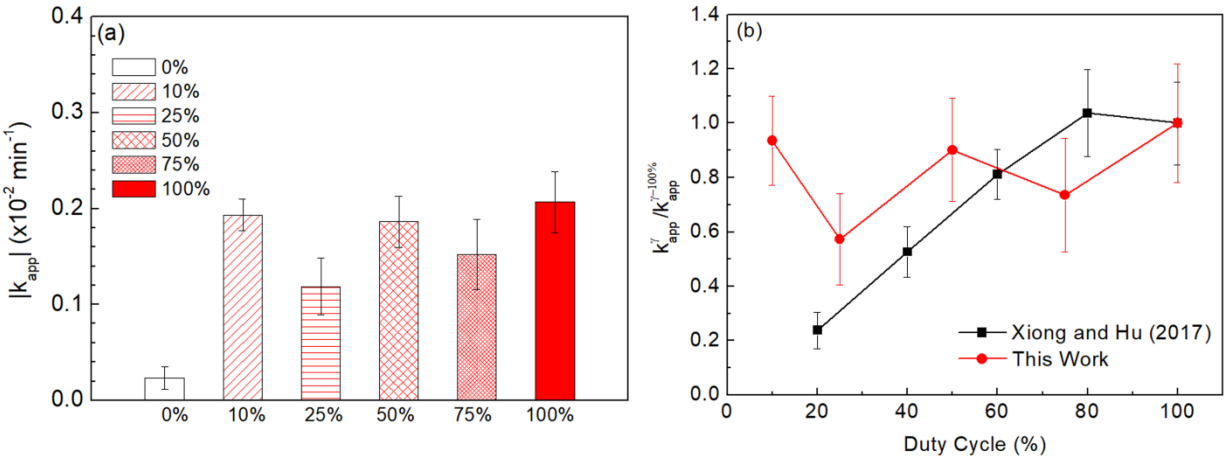

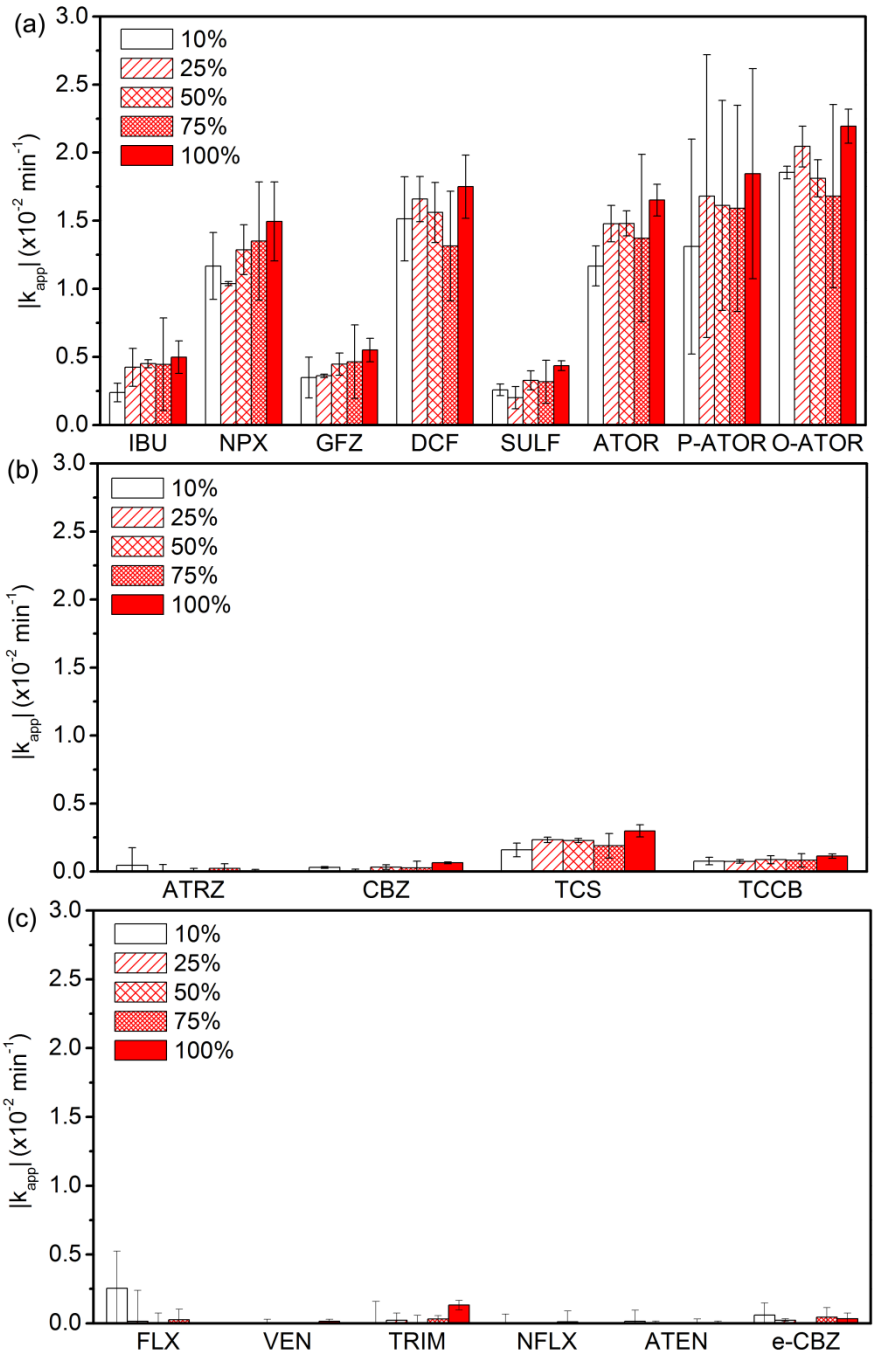
(a)
10%
25%
50%
75%
100%
$|k_{app}|$ ($x10^{-2}$ min^{-1})
3.0
2.5
2.0
1.5
1.0
0.5
0.0
IBU
NPX
GFZ
DCF
SULF
ATOR
P-ATOR
O-ATOR
(b)
10%
25%
50%
75%
100%
$|k_{app}|$ ($x10^{-2}$ min^{-1})
ATRZ
CBZ
TCS
TCCB
(c)
10%
25%
50%
75%
100%
$|k_{app}|$ ($x10^{-2}$ min^{-1})
FLX
VEN
TRIM
NFLX
ATEN
e-CBZ

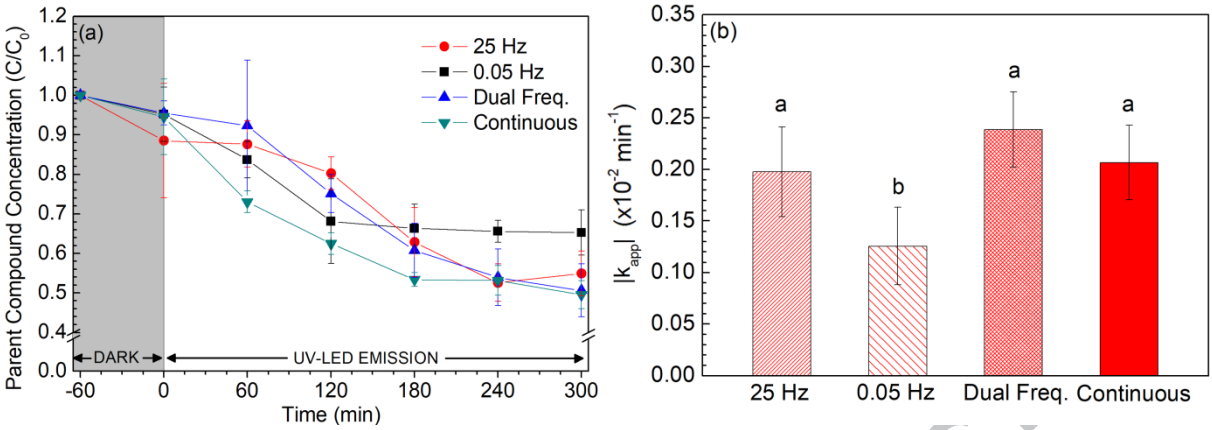

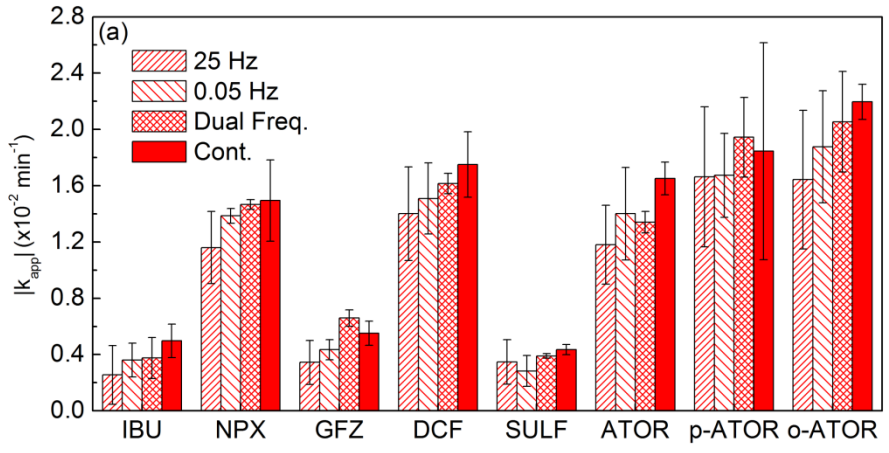

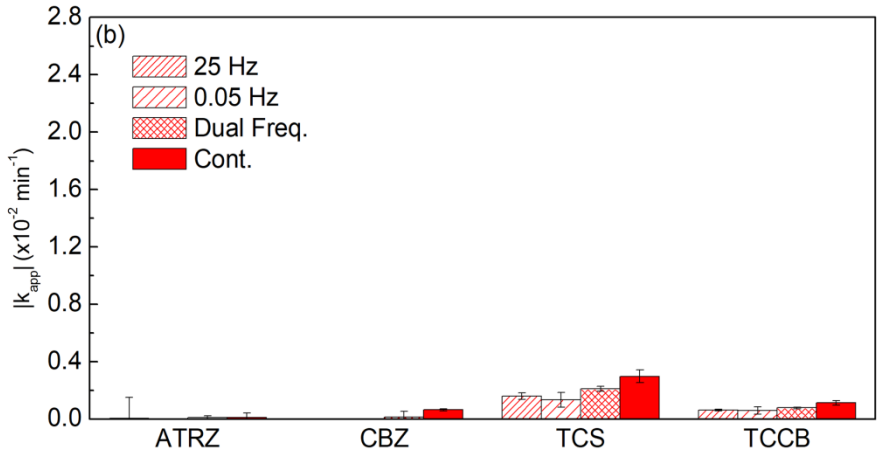

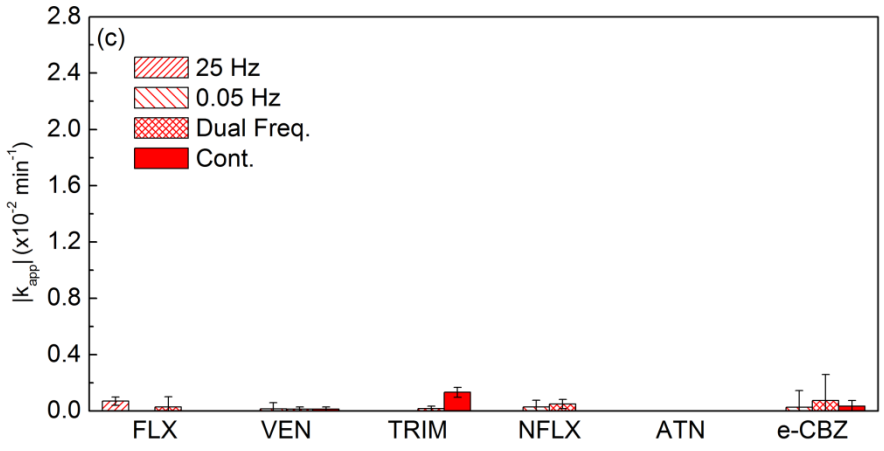

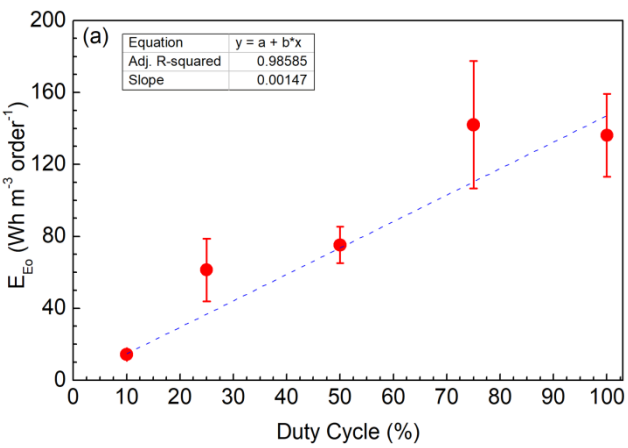

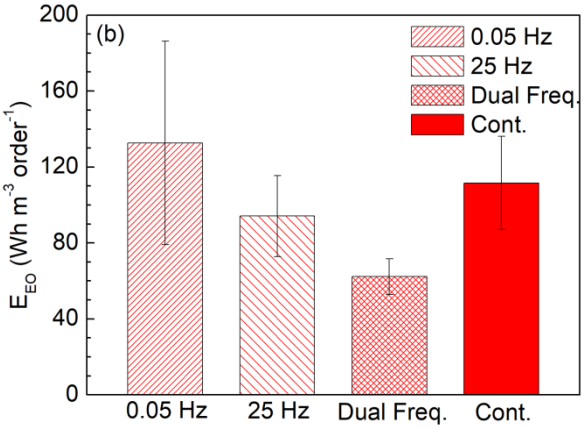

Table 1: Physical and chemical properties of target compounds.

Compound	Abbr.	Use	Mol. Weight (g mol^{-1})	pKa_1, pKa_2[a]	pIEP[a]	Net Charge Distribution Value at pH=5[a]	Solubility (logS) at pH=5[a]
Atenolol	ATEN	Beta-blocker	266.34	9.60	11.87	1(POS)	0.43
Atorvastatin	ATOR	Lipid lowering	558.64	4.33	0.98	-0.83(NEG)	-6.28
o-hydroxy atorvastatin	o-ATOR	ATOR Metabolite	573.65	4.33	0.98	-0.83(NEG)	-6.68
p-hydroxy atorvastatin	p-ATOR	ATOR Metabolite	573.65	4.33	0.98	-0.83(NEG)	-6.68
Atrazine	ATZ	Herbicide	214.68	1.6	8.74	0 (NEUT)	-3.8
Carbamazepine	CBZ	Anti-epileptic	309.33	13.9	6.10	0 (NEUT)	-3.79
Carbamazepine-10,11-epoxide	e-CBZ	CBZ Metabolite	252.27	3.65, 5.13	9.39	0.46 (POS)	-3.11
Diclofenac	DCF	Anti-inflammatory	296.15	4.51	0.96	-0.91(NEG)	-3.25
Fluoxetine	FLX	Antidepressant	309.33	9.80	11.90	1.00(POS)	<0.00
Norfluoxetine	NFLX	Metabolite	295.00	9.80	N/A	1.00 (POS)	<0.00
Gemfibrozil	GFZ	Lipid lowering agent	250.33	4.42	N/A	-0.79 (NEG)	-2.63
Ibuprofen	IBU	Anti-inflammatory	206.28	4.80	4.90	-0.58 (NEG)	-3.16
Naproxen	NPX	Anti-inflammatory	230.60	4.12	N/A	-0.87(NEG)	-2.58
Sulfamethoxazole	SULF	Antibiotic	253.28	1.6, 5.7	4.06	-0.06(NEG)	-2.17
Triclosan	TCS	Antibacterial agent	289.54	7.60	1.96	0 (NEUT)	-5.27
Triclocarban	TCB	Antibacterial agent	315.58	12.70	3.40	0 (NEUT)	-5.67
Trimethoprim	TRIM	Antibiotic	290.32	7.16	12.24	0.99 (POS)	-0.64
Venlafaxine	VEN	Antidepressant	277.40	9.8	11.66	1.00 (POS)	<0.00

pKa= acid dissociation constant, IEP = isoelectric point, S = solubility (g mol^{-1})

[a] Properties were taken from http://chemicalize.org

N/A – Not Available

Table 2: Light profiles for dark, continuous, and periodic illumination under various duty cycles (γ).

Duty Cycle (γ)	Average UV Power Intensity ($mW\ cm^{-2}$)	T_{on} (ms)	T_{off} (ms)	Period (ms)
Duty cycle experiments at constant frequency				
10%	0.22	100	900	
25%	0.54	250	750	1000 (1 Hz)
50%	1.08	500	500	
75%	1.63	750	250	
100%	2.18	----------continuous illumination----------		
Frequency experiments at constant duty cycle				
50%	1.08	10000	10000	20000 (0.05 Hz)
50%	1.08	20	20	40 (25 Hz)

T_{on} – Time light source is on; T_{off} – Time light source is off; Period – time of one exposure cycle

Table 3: Material characteristics of PTT substrate.

Material Characterization	Value	Method of Determination
Crystal Phase	Anatase	Raman Spectroscopy
Bandgap Energy	3.0 eV	Diffuse-Reflectance Spectroscopy
Surface Roughness	5-10 um	Optical Scanning
Pore Size	~10 um	Scanning Electron Microscopy
Isoelectric Point	6.0	Zeta Potential
Mass of Substrate	1.33 +/- 0.08 g	Analytical Balance

Table 4: Multiple regression analysis (forward approach).

Forwards		Model 1	Model 2	Model 3
Constant	**Slope**	0.604	-0.380	-0.285
	Std. Err.	0.113	0.239	0.190
	t	5.340	-1.591	-1.497
	p	<0.000	0.132	0.157
Net Charge	**Slope**	-0.821	-0.634	-0.924
	Std. Err.	0.153	0.114	0.127
	t	-5.361	-5.579	-7.277
	p	<0.000	<0.000	<0.000
Molecular Weight	**Slope**		0.003	0.004
	Std. Err.		<0.000	<0.000
	t		4.353	6.396
	p		<0.000	<0.000
Solubility	**Slope**			0.152
	Std. Err.			0.047
	t			3.210
	p			0.006
Adjusted R^2		0.620	0.821	0.889
Residual Sum of Squares		3.68	1.628	0.938

Highlights

- 18 PPCPs were decomposed by an advanced oxidation process using UV-LEDs.
- The TiO_2 catalyst was immobilized on a porous Ti substrate.
- Kinetic rates of PPCPs were explained by factors like charge, solubility, and molecular weight.
- Negative PPCPs had the highest removal due to electrostatic attraction to the positive substrate.
- Using controlled periodic illumination to decrease the energy usage did not sacrifice PPCP removal performance.